

AD-A061 944

NAVAL RESEARCH LAB WASHINGTON D C
A PERSPECTIVE SELF-GENERATED MAGNETIC FIELDS. (U)
OCT 78 J A STAMPER
NRL-MR-3872

F/G 20/9

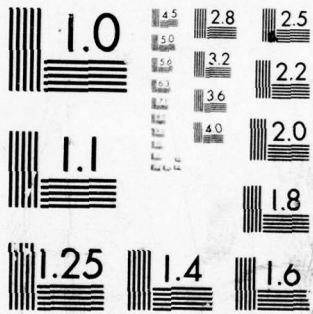
UNCLASSIFIED

NL

1 OF 1
AD
A061 944



END
DATE
FILMED
2--79
DDC



MICROCOPY RESOLUTION TEST CHART
NATIONAL BUREAU OF STANDARDS-1963-A

125c

NRL Memorandum Report 3872

AD A061944

A Perspective on Self-Generated Magnetic Fields

J. A. STAMPER

*Laser Plasma Branch
Plasma Physics Division*

LEVEL

DDC FILE COPY

October 27, 1978



DDC
RECEIVED
DEC 8 1978
A

NAVAL RESEARCH LABORATORY
Washington, D.C.

Approved for public release; distribution unlimited.

78 12 08 027

9 Memorandum reply

SECURITY CLASSIFICATION OF THIS PAGE (When Data Entered)

REPORT DOCUMENTATION PAGE		READ INSTRUCTIONS BEFORE COMPLETING FORM
1. REPORT NUMBER NRL Memorandum Report 3872	2. GOVT ACCESSION NO.	3. RECIPIENT'S CATALOG NUMBER
4. TITLE (and Subtitle) 6 A PERSPECTIVE ON SELF-GENERATED MAGNETIC FIELDS	5. TYPE OF REPORT & PERIOD COVERED Interim report on a continuing NRL Problem	
7. AUTHOR(s) 10 J. A. Stamper	6. PERFORMING ORG. REPORT NUMBER	
9. PERFORMING ORGANIZATION NAME AND ADDRESS Naval Research Laboratory Washington, D. C. 20375	8. CONTRACT OR GRANT NUMBER(s) 14 NRL-MR-3872	
11. CONTROLLING OFFICE NAME AND ADDRESS Department of Energy Washington, D. C. 20545	10. PROGRAM ELEMENT, PROJECT, TASK AREA & WORK UNIT NUMBERS 67H02-29A	
14. MONITORING AGENCY NAME & ADDRESS (if different from Controlling Office) 12 42 p.	12. REPORT DATE 11 27 October 1978	
	13. NUMBER OF PAGES 41	
	15. SECURITY CLASS. (of this report) UNCLASSIFIED	
	15a. DECLASSIFICATION/DOWNGRADING SCHEDULE	
16. DISTRIBUTION STATEMENT (of this Report) Approved for public release; distribution unlimited.		
17. DISTRIBUTION STATEMENT (of the abstract entered in Block 20, if different from Report)		
18. SUPPLEMENTARY NOTES Work performed at the Naval Research Laboratory under the auspices of the Department of Energy.		
19. KEY WORDS (Continue on reverse side if necessary and identify by block number) Magnetic field Self-generated Laser-fusion Radiative effects		
20. ABSTRACT (Continue on reverse side if necessary and identify by block number) Self-generated magnetic fields in the megagauss range have recently been re-confirmed by Faraday rotation diagnostics of laser-plasma coupling. These fields, through their inhibition on thermal transport, could have an important effect in pellet design. There has been impressive progress over the last decade, both experimentally and theoretically, toward understanding the physics of the magnetic fields. The newer results can be seen in the historical perspective of the many past contributions described in the published literature. Direct experimental studies have utilized both physical probes (coils) and Faraday rotation of a polarized, probing laser beam. (Experimental x-ray (Continued) next page		

DD FORM 1 JAN 73 1473

EDITION OF 1 NOV 65 IS OBSOLETE
S/N 0102-014-6601

SECURITY CLASSIFICATION OF THIS PAGE (When Data Entered)

251 950

Lee

20. ABSTRACT (Continued)

studies have also provided indirect evidence for the fields by requiring thermal transport inhibition in a self-consistent 2-D numerical modelling of the laser-plasma interactions.) The rich variety of theoretical studies includes magnetic field effects in ordinary and magnetic resonant absorption. A 3-channel diagnostic system, utilizing Faraday rotation of a Raman-shifted beam, has allowed a study of the magnetic field dependence on several experimental conditions—particularly timing and the presence of a pre-formed plasma. Future work includes determining the importance of the fields at the lower irradiances now under consideration for pellets, and measuring the fields in the critical region where resonant absorption and radiative forces are important.

CONTENTS

I. INTRODUCTION 1

II. THEORETICAL BACKGROUND 4

III. STUDIES OF SELF-GENERATED MAGNETIC FIELD EFFECTS 6

VI. EXAMPLES OF MAGNETIC FIELD EFFECTS 9

V. DIRECT EFFECTS OF THE LASER RADIATION 11

VI. FARADAY ROTATION EXPERIMENTS 18

VII. CONCLUSION 31

VIII. ACKNOWLEDGMENTS 31

REFERENCES 33

ADDRESSING SLIP	
RY76	White Section <input checked="" type="checkbox"/>
EDC	Dark Section <input type="checkbox"/>
UNANNOUNCED	<input type="checkbox"/>
JUSTIFICATION.....	
BY.....	
DISTRIBUTION / AVAILABILITY CODE	
Dist.	AVAIL. NO. OF COPIES
A	

A PERSPECTIVE ON SELF-GENERATED MAGNETIC FIELDS

I. INTRODUCTION

Self-generated magnetic fields in the megagauss range¹ have recently been re-confirmed^{2,3} by Faraday rotation diagnostics of laser-plasma interactions. These fields, through such effects as thermal transport inhibition, could have an important effect on pellet design for inertial confinement fusion. This report is based on an invited talk given at the 1978 meeting of the Plasma Physics Division of the American Physical Society. It is intended to give a current perspective, based on the author's experience, of the experimental and theoretical work on self-generated magnetic fields. The discussion will first consist of a brief historical and heuristic review with references to much of the published work. This will be followed by a more detailed discussion of recent experimental work at the Naval Research Laboratory.

a. Relation to Laser Pulse Character

In studying the physics relevant to inertial confinement fusion by lasers, a short, powerful pulse of laser radiation is focused to a small diameter onto a solid target. The resulting laser-produced plasma is observed to contain a large magnetic field, produced directly as a result of the laser-plasma interaction. This is the "self-generated" or "spontaneous" magnetic field which will be discussed. The implied large magnetic field generation rate was, at first, quite surprising but is, in fact, a direct consequence of the character of the laser pulse.

Manuscript submitted October 23, 1978.

The laser-produced plasma can be roughly represented, as shown in Fig. 1, by a cylinder of radius r (determined by laser focal radius) and thickness w . The laser-plasma interaction can then be modeled as an electric circuit.⁴ One can write $V = IR + Ldi/dt$ where the voltage V is the energy per unit charge kT/e , the resistance is $R = \rho w/\pi r^2$ (ρ = resistivity) and the inductance $L = w/c^2$. The capacitive drop can be neglected.⁴ Further, the resistive drop for a hot plasma can be neglected since $L(di/dt)/IR \sim \pi r^2/c^2 \rho \tau \gg 1$ where τ is the laser pulse width. Basically then, because of the small radius, high temperature and short pulse width, the reactance is inductive. This is the reason for the large magnetic field generation. We have $di/dt \sim kT/eL \sim c^2 kT/ew$ and, using Ampere's Law $B = 2I/rc$, gives

$$\frac{dB}{dt} \sim \frac{2c}{e} \frac{kT}{rw} \quad (1)$$

Thus, the high intensity (large kT), short pulse onto a solid target (small w) when tightly focused (small r) produces a very large field generation rate.

b. *Earlier Studies*

The earlier observations were made with physical magnetic probes, i.e., small induction coils placed near the target. Voltages, induced in the coil as the magnetic field structure expanded past the coil, were recorded on an oscilloscope. The fields were first reported in the Russian literature — both for a gas breakdown⁵ and for a solid target.⁶ Rather large fields (kilo-gauss) were reported in 1971⁷ and explained in terms of thermal sources^{7,8} — to be discussed later. It became apparent that very large fields (megagauss) could exist in the laser focal region and that they could affect the physics of laser-fusion in a variety of ways.

c. *Relevance to Laser-Fusion*

Most experiments and many of the numerical studies have been for a single laser beam focused onto a planar target. However, in laser-fusion applications, multiple beams are focused

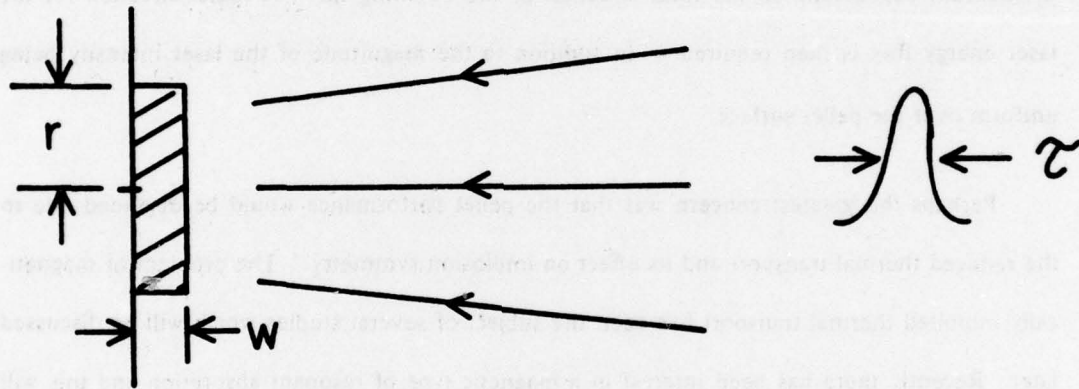


Fig. 1 - Circuit analogy for laser-produced plasma.

as uniformly as possible onto a spherical pellet. Hopefully, with reasonably uniform illumination to minimize tangential gradients, the magnetic complications will be minimized. Nevertheless, there is reason to be cautious. A 5% laser intensity variation could reduce the yield by an order of magnitude if classical transport is valid.⁹ Also, as discussed later, fields could grow, as a result of a field generating instability, from small tangential perturbations in the temperature. At higher ($\geq 10^{15}$ W/cm²) laser intensities, where the direct effects of the laser radiation are important, field generation depends (through such mechanisms as resonant absorption and field momentum deposition) on the local direction of the Poynting flux. A radial direction for the laser energy flux is then required — in addition to the magnitude of the laser intensity being uniform over the pellet surface.

Perhaps the greatest concern was that the pellet performance would be degraded due to the reduced thermal transport and its effect on implosion symmetry.⁹ The problem of magnetically inhibited thermal transport has been the subject of several studies which will be discussed later. Recently there has been interest in a magnetic type of resonant absorption and this will be discussed along with several references. The production of super-thermal electrons⁴ and their role in pre-heating the pellet core are both affected by magnetic fields. Recent studies (shocks,¹⁰ accelerated structure,¹¹ compression¹²) have been made which relate specifically to an imploding pellet. Most of the work has been concerned with the rather high irradiances (10^{15} – 10^{17} W/cm²) considered for earlier pellet designs. The role of the magnetic fields has yet to be assessed quantitatively for the lower irradiances (10^{13} – 10^{14} W/cm²) now under consideration for pellets.

II. THEORETICAL BACKGROUND

The original theories were concerned with the time development, including generation, of the magnetic field. The basic equation was dependent, through Faraday's law, on the electric

field \mathbf{E} in a laser-produced plasma. The electric field is commonly evaluated from a generalized Ohm's law which is dependent on the various forces acting on the electron fluid.

$$nm \frac{d\mathbf{V}_e}{dt} = -ne \left(\mathbf{E} + \frac{1}{c} \mathbf{V}_e \times \mathbf{B} \right) - \nabla \cdot \mathbf{P}_e + \mathbf{f}^c + \mathbf{f}^r \quad (2)$$

This is reasonable since, due to the small electron inertia, various forces acting on the electron fluid tend to be balanced with the electrical force, $-ne\mathbf{E}$. The collisional force \mathbf{f}^c is the sum of the resistive drag $\rho \cdot \mathbf{J}$ and thermal force $\alpha \cdot \nabla T$. The plasma resistivity and thermoelectric power are denoted, respectively, by ρ and α . The radiative force \mathbf{f}^r , due directly to correlations in the high frequency quantities associated with the electromagnetic fields of the laser radiation, will be discussed later.

Ignoring the electron inertia (left hand side) and using Eq. (2) in Faraday's law $\partial\mathbf{B}/\partial t = -c\nabla \times \mathbf{E}$ gives

$$\frac{\partial\mathbf{B}}{\partial t} = \nabla \times (\mathbf{V}_e \times \mathbf{B}) - \frac{c^2}{4\pi} \nabla \times [\rho \cdot (\nabla \times \mathbf{B})] + \mathbf{S} \quad (3)$$

This is the equation governing the development of the magnetic field. The first term describes convection of the magnetic field with the plasma and also, since $\mathbf{V}_e = \mathbf{V} - \mathbf{J}/ne$, includes the Hall term. The second term (through Ampere's law $\nabla \times \mathbf{B} = (4\pi/c)\mathbf{J}$) describes diffusion of the magnetic field with respect to the plasma. The last term \mathbf{S} is the magnetic source term, describing magnetic field generation. It can be expressed as $-c\nabla \times \mathbf{E}_0$ where \mathbf{E}_0 is the (initially) non-magnetic field dependent part of \mathbf{E} .

$$\mathbf{E}_0 = -\frac{1}{ne} \nabla P_e + \alpha \cdot \nabla T + \frac{\mathbf{f}^r}{ne} \quad (4)$$

The first two terms due to electron pressure and the thermal force, are responsible for the thermal source term. The usually dominant term, leading to the well-known $\nabla T \times \nabla n$ source, is the one due to electron pressure. Using $P_e = nkT$ in $\mathbf{S}_1 = -c\nabla \times \mathbf{E}_0$, where $\mathbf{E}_0 = -(1/ne)\nabla P_e$, gives

$$S_r = \frac{ck}{ne} \nabla T \times \nabla n. \quad (5)$$

This will be used later in theoretical discussions and interpreting the Faraday rotation experimental results. However, contributions due to the thermal force and radiative force will also be pointed out.

It should be recognized that Eq. (3) allows a wide range of physical phenomena to affect the production of magnetic fields. The reader who would like a more detailed, but still heuristic, discussion of the magnetic fields can refer to several of the published RPI Summer Workshop lectures.¹³⁻¹⁷ These discussions are complementary to those in the journal publications. For example, the dynamo effect (conversion of plasma flow energy to magnetic field energy) is discussed in Ref. (15)). Also, the existence of non-adiabatic electron conditions and its relevance to the thermal source is discussed on page 286 of Ref. (13) — and corrected on page 734 of Ref. (16). The role of refraction is discussed on page 729 of Ref. (17),

The thermal source, Eq. (5) is equivalent (to within a factor of 2) to the generation rate, Eq. (1), described by an inductive reactance. Consider a laser beam focused at normal incidence onto a solid target. The temperature gradient has a large component directed radially in toward the laser axis while the density gradient is directed axially into the target. Thus, with a radial scale length r and an axial scale length w , one can use $|\nabla T| \sim T/R$ and $|\nabla n| \sim n/w$ in Eq. (5) and compare with Eq. (1). The azimuthal character and direction as well as the rough magnitude of the magnetic field described by this simple model have been verified by experimental studies.

III. STUDIES OF SELF-GENERATED MAGNETIC FIELD EFFECTS

a. *Measurements with Physical Probes*

Earlier studies, utilizing physical magnetic probes, showed the azimuthal character.^{7,18} the dependence on background pressure,¹⁸ and that some field generation occurred in the expand-

ing plasma front.¹⁸ The generation was affected by the ambient plasma, continuing after the laser pulse and even reversing.¹⁹ A small early-time field component was observed for a metallic target and explained, as predicted earlier,⁴ in terms of thermionic electron emission during the laser pulse.²⁰ Despite the involvement of the background, work by Drouet and co-workers, utilizing a current probe,²¹ was consistent with the field source being at the plasma-target interface. However, the current induced in a CO₂ laser-plasma did show a resonance with background pressure.²² Their studies also showed the roles of background photoionization and magnetic field diffusion.²³ The magnetic field expansion was recently characterized by diffusion in the photoionized background followed by convection with the laser plasma.²⁴ Recent studies²⁵ also showed, as earlier,²⁰ that the magnetic field expanding from a metallic target has a fast component (due to an electron stream) as well as the component traveling with the front velocity. Probes with a subnanosecond response have shown that the rise of the magnetic field is synchronous with the initial formation of the plasma.²⁶

Thus, although studies using physical (magnetic and current) probes have shown the involvement of the target in field generation²¹ and that the rise is synchronous with the laser pulse,²⁶ these probes are not able to directly sample the laser-plasma interaction region — in the focus of the laser. This is the region of large thermal sources (Eq. (5)) which have played an important role in our theoretical understanding of the magnetic fields and which could have an important effect in laser-fusion applications.⁹ Magnetic fields have been measured in the laser focal region^{1,2,3} with Faraday rotation diagnostics and a detailed description of one of these studies² is given later.

b. *Numerical Studies — Thermal Transport Inhibition*

Our understanding of the magnetic fields has depended heavily on numerical studies with a thermal source. The importance of magnetically inhibited thermal transport was apparent

from early comparison with experiment. It was shown that including the fields, in a 2-D simulation of experiments on a deuterium plasma, gave a hotter plasma, more neutrons and better agreement with experiment.²⁷ Numerical simulations were also used in developing analytic expressions for the magnetic field.²⁸ Studies on an aluminum plasma showed that the fields played an important role in determining the conversion efficiency from laser-energy to plasma radiation.²⁹ Later 2-D studies³⁰ on aluminum included the full magnetic effect on the transport coefficients, atomic rate equations, and radiation transport with frequency diffusion. There was good agreement with experimental x-ray spectra and conversion efficiency.

Magnetically inhibited thermal transport has usually been treated with a laminar theory, either with classical or Bohm rates. However, it has been pointed out that a small-scale, disordered structure in the magnetic field would enhance the cross-field thermal transport above the classical value although transport would still be strongly inhibited over the non-magnetic value.³¹

Comparisons of the absolute x-ray spectra observed from slabs³² of polyethylene (CH_2) or small discs³³ of parylene (C_5H_8) with 2-D simulations showed good agreement only when magnetic effects (thermal inhibition) were self-consistently included. Further, for the parylene discs,³³ the observed spatial distribution of x-ray emission transverse to the beam axis agreed with simulations only when thermal inhibition was included. Simulations have also shown that B-field thermal inhibition can produce local "hot spots"³⁴ which could play a role in energetic ion production.

c. *Composition Discontinuities*

The thermal source can be very large in the presence of a composition discontinuity.³⁵ For example, such discontinuities exist at the boundaries in multi-layer pellets and their effect in

pellet compression and expansion has been studied.¹² Also, the magnetic turbulence associated with the discontinuities at impurity grains³⁶⁻³⁸ could have application in coupling a target plasma to a relativistic electron beam. The negative result, reported in Ref. (3) is not conclusive since the target and experimental conditions may not have been well suited for observing the composition discontinuity effect.

IV. EXAMPLES OF MAGNETIC FIELD EFFECTS

The problem of thermal transport inhibition due to self-generated magnetic fields has, as evidenced by the studies in Section III-b, received considerable attention. However, the other magnetic effects on transport can also be important. The magnetic field introduces, through the Lorentz force, skew — symmetric components in the transport tensors. There is thus an explicit dependence on the magnetic field in the form of a cross-product with the field. This is illustrated by two effects which occur in the presence of a temperature gradient.

There is a contribution to the heat flux (analogous to the Righi-Leduc effect in solids) which depends on the cross-product of the magnetic field with the temperature gradient.

$$\mathbf{q} = \frac{-K_{\perp}}{B} \mathbf{B} \times \nabla T \quad (6)$$

The cross thermal conductivity K_{\perp} is positive. It is assumed that ∇T and ∇n are initially parallel and that a small perturbation $\nabla_{\perp} T$ is introduced which is perpendicular to ∇n . The resulting thermal source (Eq. (5)) can then be combined with Eq. (6) to give a heat flux along $(\nabla T \cdot \nabla n) \nabla_{\perp} T$. When density and temperature vary in the same direction ($\nabla T \cdot \nabla n > 0$), heat will flow into the hotter region-increasing the perpendicular temperature gradient and thermal source term. This is the field generating thermal instability which has been described in the literature.³⁹⁻⁴¹ It has been seen in numerical simulations by McCrory.⁴²

78 12⁹ 08 027

An interconversion between thermal and magnetic energy has also been described as the basis for a type of travelling wave, called a thermal-magnetic wave.⁴³ These waves could be viewed as an oscillation between particle and magnetic field energy. The particle to field conversion is due to the thermal source, and the field to particle conversion is due to current flow through the ambipolar field. As a result of current flow parallel to an electric field, field energy is converted to particle energy at a rate $\mathbf{E} \cdot \mathbf{J}$. Using the ambipolar field $\mathbf{E}_0 = -(1/ne)\nabla P$ (also responsible for the thermal force), $\mathbf{J} = (c/4\pi)\nabla \times \mathbf{B}$, assuming T varies slowly compared to n and letting $\beta = -\ln(n)$ gives a conversion rate to electron energy density $\epsilon = (3/2)nKT$ as

$$\frac{\partial \epsilon}{\partial t} = \frac{ckT}{4\pi e} \nabla \beta \cdot (\nabla \times \mathbf{B}) \quad (7)$$

However, for the $\mathbf{E}_0 \cdot \mathbf{J}$ conversion to be applicable, there must be some mechanism for a rapid and local thermalization. When \mathbf{B} is azimuthal ($\mathbf{B} = B(r, z)\hat{\theta}$), and n, β are functions of radius only, then Eq. (7) becomes $\partial \epsilon / \partial t = -(ckT/4\pi e) (d\beta/dr) (\partial B/\partial z)$. Using this with the equation, $\partial B/\partial t = -(2c/3ne) (d\beta/dr) (\partial \epsilon/\partial z)$, for a thermal source (Eq. (5)) shows that small perturbations in ϵ or B travel along surfaces of constant density with a phase velocity $V_p = (c/\omega_p) (d\beta/dr) \sqrt{2kT/3m}$. This agrees (within a factor of $\sqrt{2/3}$) with the velocity of thermal-magnetic waves given in Ref. (43). The ratio of V_p to the electron thermal velocity is approximately the ratio of the collision-free skin depth c/ω_p ($.17 \mu\text{m}$ at 10^{21}cm^{-3}) to the density scale length. It was noted in Ref. (43) that the energy flux associated with these waves could be important when magnetic thermal transport inhibition was large.

The other effect to be discussed involves a contribution to the electric field which depends on the cross-product of the magnetic field with the temperature gradient. This is analogous to the Nernst effect in solids, i.e., the magnetic part of the thermal force.

$$\mathbf{E}_N = - Q\mathbf{B} \times \nabla T \quad (8)$$

Using this expression for the Nernst electric field in Faraday's law shows that the magnetic field growth rate has a dominant term that varies as $cQB\nabla^2 T$. The Nernst coefficient Q is positive. Thus, at radii greater than that of the temperature inflection point, the fields will be enhanced — and they will be reduced at smaller radii. The net result of the Nernst effect is that the dominant fields tend to occur at larger radii. Numerical studies by Colombant and Winsor⁴⁴ showed that inclusion of the thermal force caused the magnetic field maxima to be shifted to larger radii and later times. These studies also showed that the thermal force smoothed out the spatial and temporal variations of the magnetic field. This general feature is consistent with the results of the Faraday rotation study which will be described later.

V. DIRECT EFFECTS OF THE LASER RADIATION

a. Background Discussion

There has been interest recently in magnetic field effects due directly to time-correlations in the high frequency quantities associated with the electro-magnetic (e.m.) fields of the laser radiation. These high-frequency e.m. fields $\delta\mathbf{E}$, $\delta\mathbf{B}$ induce high frequency velocity $\delta\mathbf{v}$ and density δn oscillations in the electrons. One can define several low frequency or time-averaged $\langle \rangle$ products of the high-frequency quantities which are of interest. In particular, one can define a field pressure $P = \langle (\delta\mathbf{E})^2 \rangle / 8\pi$, field momentum density $\mathbf{g} = \langle \delta\mathbf{E} \times \delta\mathbf{B} \rangle / 4\pi c$ and a current density $\mathbf{J}_w = -e \langle \delta\mathbf{v} \delta n \rangle$ driven by the laser radiation. This current will be called the wave current since it involves the coherent action of plasma waves.

The low frequency radiative force \mathbf{f}' on the electrons can then be expressed as⁴⁵

$$\mathbf{f}' = (\epsilon_r - 1)\nabla P + \epsilon_r \omega \mathbf{g} + \epsilon_r (m\nu/e)\mathbf{J}_w \quad (9)$$

where ω and ν are the laser and effective collision frequencies and ϵ_r and ϵ_i are the real and imaginary parts of the dielectric function. The first term is the ponderomotive force which, through density profile modification,⁴⁶⁻⁴⁹ has an appreciable effect on the laser-plasma interactions. The second term represents the force on the plasma due to field momentum deposition during absorption. It is in the direction of the Poynting flux $\mathbf{I} = c^2 \mathbf{g}$ and can be expressed as $K \bar{n} / c$ where the absorption coefficient K is given by $\bar{n} [1 + (\nu/\omega)^2]$ $K = (\omega_p/\omega)^2 (\nu/c)$ and $\bar{n} = \sqrt{\epsilon_r}$ is the refractive index.

The last term includes the effects of a resistive drag due to the wave current. The (corrected) term $(\epsilon_i/8\pi) \text{Im}(\mathbf{E}^* \nabla \cdot \mathbf{E})$, given only in the text of Ref. (45), was derived from the force $-\nabla \cdot \mathbf{P}$ due to radiation pressure. It can be expressed as the resistive drag $(m\nu/e) \mathbf{J}'_w$ of a wave current $\mathbf{J}'_w = (1 - \epsilon_r) e \langle \delta n \delta \mathbf{v} \rangle$. However, as pointed out by Woo and DeGroot,⁵⁰ this would be nearly canceled by the resistive drag $(m\nu/e) \mathbf{J}_w$ (omitted in Ref. (45)) due to the current $\mathbf{J}_w = -e \langle \delta n \delta \mathbf{v} \rangle$ directly involving the high frequency density δn . The current $\mathbf{J}'_w = (n/n_{cr}) \mathbf{J}_w$ agrees (through Ampere's law) with the steady magnetic field (Eq. (1)) in Ref. (53). The last term of our Eq. (9) includes both contributions and may be small since ϵ_r is small near the critical density and \mathbf{J}_w is small elsewhere.

The current \mathbf{J}_w , driven coherently by the laser radiation, is important in resonant absorption which is discussed later. However, a current \mathbf{J}_r can also be driven by the laser radiation through random velocity dependent phase-shifts (due to collisions or plasma wave turbulence). The associated resistive drag force can be expressed as $(m\nu/e) \mathbf{J}_r$ where the effective collision frequency ν is given by $\epsilon_i \omega = (1 - \epsilon_r) \nu = (n/n_{cr}) \nu$. When the drag force is balanced with the force $\epsilon_i \omega \mathbf{g}$ due to field momentum deposition then one can express \mathbf{J}_r as $-(e/m) (n/n_{cr}) \mathbf{g}$. This current is, itself, independent of ν and can be written as $-ne \mathbf{V}_d$ where \mathbf{V}_d is a collision-free drift velocity. One can express V_d/c as the ratio of Poynting flux \mathbf{I} to an electron energy

flux $n_e mc^3$ ($\sim 2.4 \times 10^{18}$ W/cm² at 1.064 μ m). It is curious that, as shown next, one can also express V_d as the electron drift due to a collision-free "magnetic" radiative force.

Plasma inhomogeneity and dissipation ($\epsilon_i \neq 0$) are the mechanisms leading to the radiative forces in Eq. (9). A steady magnetic field \mathbf{B}_0 also acts as a (collision-free) mechanism for a radiative force.⁵¹ Let us consider a linearly polarized laser beam propagating, perpendicular to \mathbf{B}_0 , into a homogeneous, collision-free plasma. Then the electrons are subject to a time-averaged magnetic radiative force

$$\mathbf{f}_b = - \left(\frac{\omega_p}{\omega} \right)^2 \frac{\omega_c}{c} \frac{I}{c} (\hat{b}_0 \cdot \hat{b}) \hat{e} \quad (10)$$

where the unit vectors \hat{b}_0 , \hat{b} , \hat{e} are, respectively, along \mathbf{B}_0 and the oscillating magnetic and electric fields, ω_p is plasma frequency, ω_c is cyclotron frequency (eB_0/mc) and I is the magnitude of the laser irradiance or Poynting flux. An approximate cancellation of the magnetic force with a $\nabla \times \mathbf{u}_d$ term was reported for a calculation in the second part of Ref. (50). This may mean that the magnetic force does not contribute significantly to its own magnetic field. However, the cancellation is not general since the magnetic force exists even in a homogeneous magnetized plasma where the $\nabla \times \mathbf{u}_d$ term vanishes. A derivation based on the upper-hybrid or extraordinary mode shows that $(\omega_p/\omega)^2$ should be replaced by a resonant factor $\omega_p^2/(\omega^2 - \omega_{UH}^2)$ when near (but not at) the upper hybrid resonance.⁵² When $\hat{b}_0 \cdot \hat{b} = 1$, the magnetic drift $(\mathbf{f}_b/ne) \times \mathbf{B}_0/B_0^2$ of an electron subject to the magnetic radiative force Eq. (10), is the collision-free drift velocity V_d discussed previously. It should be noted that V_d is independent of B_0 .

The direct effects of the laser radiation have required a generalization of how the magnetic fields are treated. Originally, the explicit time variation was treated through Faraday's law and the emphasis was on magnetic field "generation." As pointed out earlier, the radiative force

gives a contribution f'/ne to the field \mathbf{E}_0 determining the generation rate $-c\nabla \times \mathbf{E}_0$. However, the wave current \mathbf{J}_w , driven coherently by the laser radiation, has a separate and direct contribution through Ampere's law.⁵³ As discussed earlier, the wave current resistive drag may be only a small contribution to the radiative force and thus to the magnetic field generation or the explicit time dependence. However, in resonant absorption, the wave current itself plays a dominant role so that the dominant time variation may be that implicit in the dependence of \mathbf{J}_w on the time-varying magnitude of the high-frequency electric field. One should note that \mathbf{J}_w does not involve a time-averaged electron velocity. Only the usual drift current $\mathbf{J}_0 = ne(\mathbf{V} - \mathbf{V}_e)$, involving time-averaged plasma and electron velocities, is related to convection of the magnetic field. Also, one can no longer simply incorporate, via Ampere's law, the total current $\mathbf{J}_0 + \mathbf{J}_w$ resistive drag force into the field diffusion term since different resistive drags are required for the drift and wave currents. The general problem has not yet been treated although extensive work has been done on resonant absorption.

b. *Radiative Effects in Magnetic Field Generation*

It was pointed out in 1973 that magnetic field generation was expected due directly to the forces associated with laser radiation pressure.⁵⁴ The first paper on the magnetic fields associated with resonant absorption showed that there was a very large field generation rate and described the geometry of the fields.⁵⁵ Field momentum deposition was described in 1976 as a mechanism for magnetic field generation.⁴⁵ However, the example in Ref. (45) of resonant absorption was not appropriate since the principal mechanism in resonant absorption is the wave current rather than field momentum deposition. In fact, field generation as an isolated concept is not so useful for magnetic fields driven coherently by the laser radiation.⁵³ The generation of a current (and thus magnetic field) driven by the dissipation of Poynting flux was also described as a mechanism in Ref. (56). This current is the one \mathbf{J}_R , given in Section V-a, resulting from

a balance of the resistive drag force with the radiative force due to field momentum deposition.⁴⁵

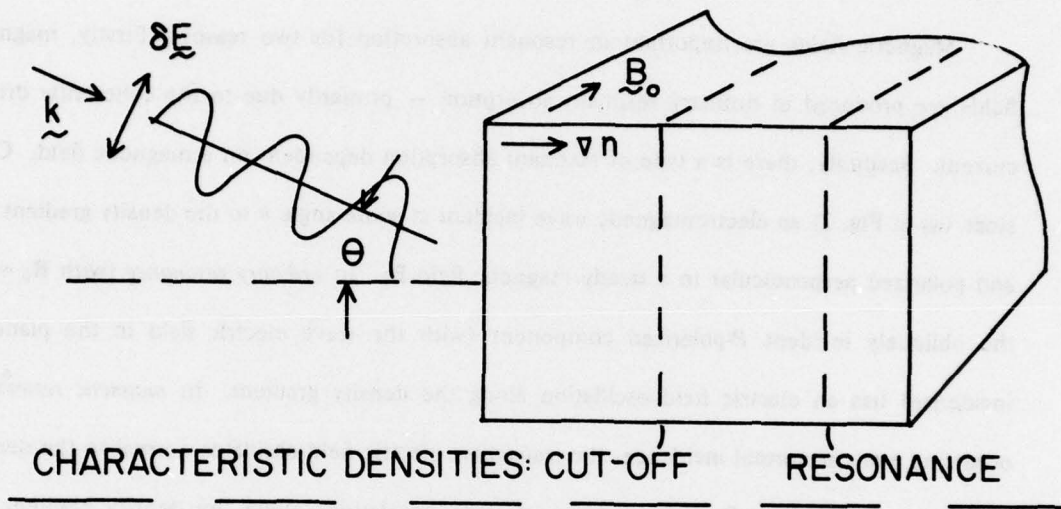
c. Discussion of Resonant Absorption

Magnetic fields are important in resonant absorption for two reasons: Firstly, magnetic fields are produced in ordinary resonant absorption — primarily due to the coherently driven current. Secondly, there is a type of resonant absorption dependent on a magnetic field. Consider (as in Fig. 2) an electromagnetic wave incident at some angle θ to the density gradient ∇n and polarized perpendicular to a steady magnetic field \mathbf{B}_0 . In *ordinary resonance* (with $\mathbf{B}_0 = 0$), the obliquely incident *P*-polarized component (with the wave electric field in the plane of incidence) has an electric field oscillation along the density gradient. In *magnetic resonance*, occurring even at normal incidence, the transverse electric field oscillates normal to the density gradient but the $V_{0s} \times \mathbf{B}_0$ force induces electron oscillations along the density gradient. In either case, these oscillations along the density gradient produce charge separation and drive plasma waves. Transverse waves can propagate up to the appropriate cut-off density and tunnel in to drive plasma waves at the resonant density which are damped into plasma energy. Langmuir waves are involved in ordinary resonance and upper-hybrid waves are involved in magnetic resonance. Large θ or B_0 implies a large transverse electric field at cut-off while a small θ or B_0 implies a more efficient tunneling. There is thus an optimum θ or B_0 for energy transfer to the plasma. In fact, Woo, Estabrook, and DeGroot have found an optimum combination of θ and B for oblique incidence in a magnetized plasma.⁵⁷

d. Theory of Magnetic Fields Due to Ordinary Resonant Absorption

There has been a variety of studies in addition to the two mentioned earlier,^{53,55} on magnetic fields due to resonant absorption. It has been pointed out⁵⁸ that the magnetic source term

RESONANT ABSORPTION



ORDINARY: $\theta \neq 0$, $B_0 = 0$, P-POLARIZATION*
OR TM MODE.

MAGNETIC: $\theta = 0$, $B_0 \neq 0$, EXTRAORDINARY ($\delta E \perp B_0$)
OR UPPER-HYBRID MODE.

* P-POLARIZATION ($\delta E \parallel$ PLANE OF $k, \nabla n$)
S-POLARIZATION ($\delta E \perp$ PLANE OF $k, \nabla n$)

Fig. 2 - Ordinary and magnetic resonant absorption.

depends on either thermal motion or dissipation. However, it may be more meaningful to calculate the magnetic field itself; and this does not require dissipation — being due to the wave current driven by linear mode conversion under collision-free conditions.⁵⁹ A warm plasma, momentum dependent generalization of the ponderomotive potential⁶⁰ could be used for a rather general description of the field generation. Finally, it should be noted that magnetic fields are produced in the parametric decay absorption of S-polarized waves as well as the resonant absorption of P-polarized waves.⁵⁰

e. *Observations of Magnetic Fields Due to Resonant Absorption*

The laser-plasma interaction can be simulated by the interaction of intense microwaves with a large, collision-free plasma. Physical probes (coils) can then be used to study the magnetic fields. In one such study,⁶¹ self-generated magnetic fields generated in the presence of microwave radiation were observed to be perpendicular to the density gradient and incident-microwave polarization, thus being consistent with resonant absorption. In another study,⁶² the magnetic fields were found to have contributions from both resonant absorption and thermal sources. More recently,⁶³ magnetic probes have been used to study the growth, diffusion and saturation of magnetic fields due to the absorption of microwaves.

f. *The Inverse Effect: Resonant Absorption Due to Magnetic Fields*

There has also been considerable interest recently in the magnetic type of resonant absorption — involving the production and damping of upper-hybrid waves. Numerical simulations with a linear density profile⁶⁴ have shown that the absorption could be important for laser-fusion. An earlier, cold-plasma study⁶⁵ with a Budden profile also showed interesting absorption. An analytic, warm — plasma theory with a linear profile⁶⁶ predicted a 70% absorption. Finally, according to an analytic and numerical study of the combined effect, i.e., oblique incidence in a magnetized plasma, it is possible to get 99% absorption.⁶⁷

g. *Discussion of Validity of the Theory*

The radiative effects just considered were treated primarily with collision-free theory. On the other hand, our understanding of magnetic effects in experiments and laser-fusion applications have depended heavily on fluid theory-particularly 2-D numerical studies with a thermal source. However, the validity of the fluid description is questionable for experiments at high laser irradiance ($\sim 10^{16}$ W/cm²) where there is a hot electron component of around 10 keV. There is need for caution until a more general description is available.

VI. FARADAY ROTATION EXPERIMENTS

a. *Background Discussion*

Experimental studies of the very large (MG) magnetic fields which occur in the focal region of the laser must involve optical techniques. The only published measurements¹⁻³ have utilized Faraday rotation of a polarized probing laser beam. The original study¹ utilized the second harmonic (5320 Å) of the main Nd-glass laser beam. However, plasma emission at both the second and third harmonic was too intense⁶⁸ for higher irradiance ($\sim 10^{16}$ W/cm²) experiments^{2,3} that it was necessary at NRL to use a non-harmonic wavelength. Studies with small disc targets,⁶⁹ heated at a lower irradiance (10^{14} W/cm²), have been carried out at the fourth harmonic wavelength (2660 Å) but they showed no fields larger than 100 kG. This discussion will be concerned primarily with the recent study² carried out at the Naval Research Laboratory (NRL), although one interesting recent result will be presented from the Rutherford Laboratory.³

What is Faraday Rotation? A plane-polarized electro-magnetic wave propagating along a magnetic field remains plane polarized but the plane of polarization rotates as the wave propagates along its path. This is illustrated in Fig. 3 for a part of the probe beam passing above

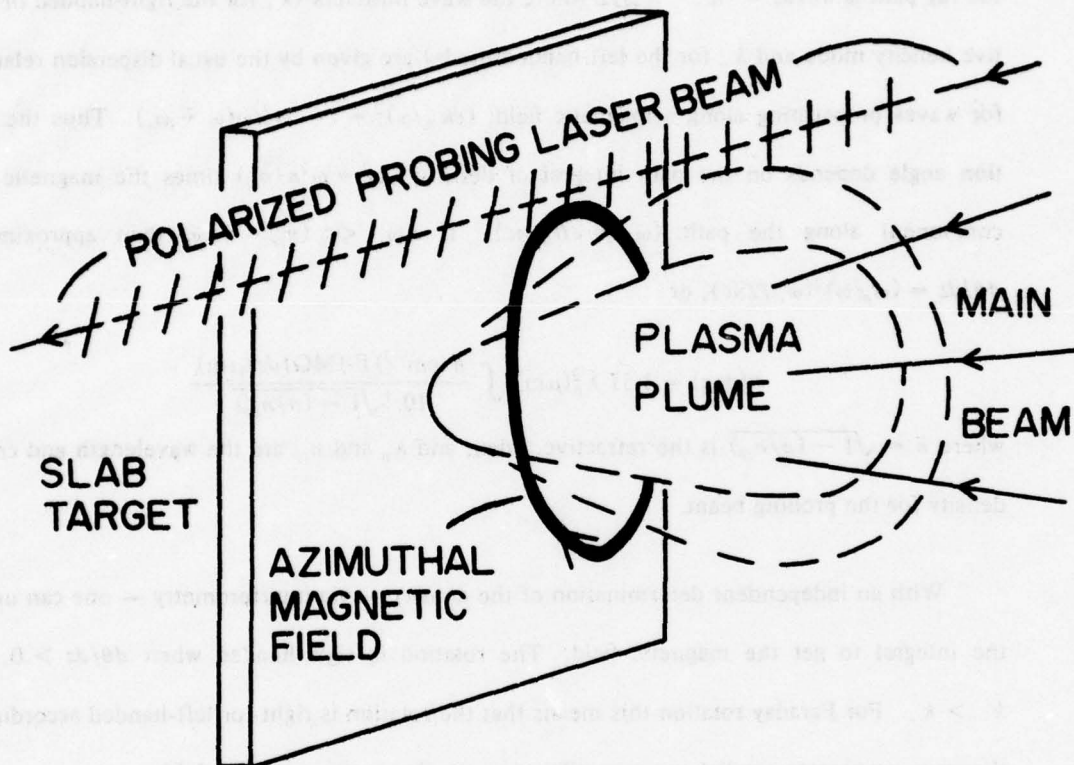


Fig. 3 - Faraday rotation of a polarized laser probing beam.

the plasma where the azimuthal magnetic field has a component along (actually, anti-parallel to) the local probe propagation direction.

The rate of change of the right-handed rotation angle θ with respect to distance z along the ray path is $d\theta/dz = (k_- - k_+)/2$ where the wave numbers (k_+ for the right-handed or positive helicity mode and k_- for the left-handed mode) are given by the usual dispersion relation⁷⁰ for waves propagating along a magnetic field: $(ck_{\pm}/\omega)^2 = 1 - \omega_p^2/\omega(\omega \mp \omega_c)$. Thus the rotation angle depends on the path integral of density ($\omega_p^2 = \omega^2 n/n_{cp}$) times the magnetic field component along the path ($\omega_c = eB_z/mc$). If $n\omega_c \ll (n_{cp} - n)\omega$, then approximately $d\theta/dz = (\omega_p/\omega)^2(\omega_c/2\bar{n}c)$, or

$$\theta(\text{deg}) = 1.51 \lambda_p^2(\mu\text{m}) \int \frac{n(\text{cm}^{-3}) B_z(\text{MG}) dz(\mu\text{m})}{10^{21} \sqrt{1 - (n/n_{cp})}} \quad (11)$$

where $\bar{n} = \sqrt{1 - (n/n_{cp})}$ is the refractive index, and λ_p and n_{cp} are the wavelength and critical density for the probing beam.

With an independent determination of the density — via interferometry — one can unfold the integral to get the magnetic field. The rotation is right-handed when $d\theta/dz > 0$, i.e., $k_- > k_+$. For Faraday rotation this means that the rotation is right- or left-handed according as the wave propagates parallel or antiparallel, respectively, to the magnetic field.

b. Experimental Set-Up

A 3-channel diagnostic system, utilizing a non-harmonic laser probing beam, was used to study the magnetic field dependence on a variety of experimental conditions — in particular, timing and the presence of pre-formed plasma. The plasma was produced, as shown at the bottom of Fig. 4, by focusing the main Nd-glass laser pulse (~ 3 to 5 J in 75 psec, FWHM) onto the target to get an irradiance just under 10^{16} W/cm². Part of the main pulse was split-off in

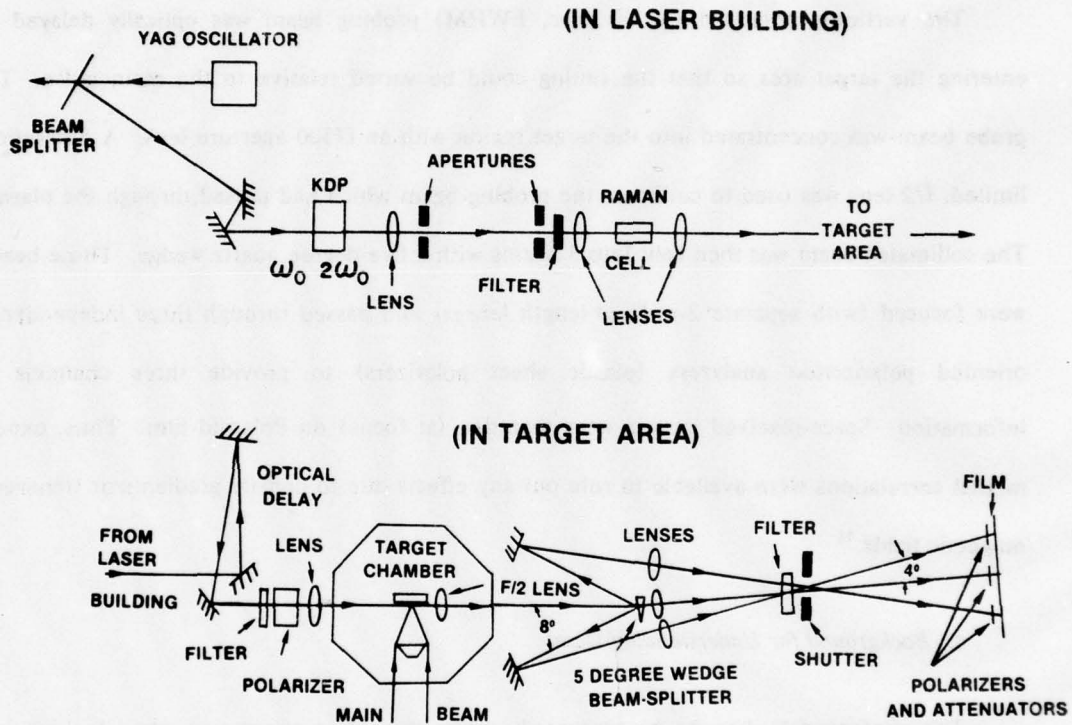


Fig. 4 - Diagram of experimental arrangement for Faraday rotation study.

the oscillator section, as shown at the top, and passed through a KDP crystal to produce the green (5320 Å) second harmonic. The collimated second harmonic beam was focused into an ethanol cell where the red (6329 Å), Raman-shifted, non-harmonic probing wavelength was produced.

The vertically polarized (~ 50 psec, FWHM) probing beam was optically delayed on entering the target area so that the timing could be varied relative to the main pulse. The probe beam was concentrated into the target region with an $f/300$ aperture lens. A diffraction-limited, $f/2$ lens was used to collimate the probing beam which had passed through the plasma. The collimated beam was then split into 3 beams with a five degree quartz wedge. These beams were focused (with separate 2-m-focal-length lenses) and passed through three independently oriented polarization analyzers (plastic sheet polarizers) to provide three channels of information. Space-resolved images were recorded (at focus) on Polaroid film. Thus, experimental correlations were available to rule out any effects due to density gradients or transverse magnetic fields.⁷¹

c. Background for Understanding Data

The photographic data, to be presented, shows the actual orientation when looking into the probing beam with the main laser beam incident from the right. This is the orientation in Fig. 5. The orientation of the thermally generated magnetic field is depicted on the left-hand side. The magnetic field is in the direction of $\nabla T \times \nabla n$ with the temperature gradient cylindrically in toward the laser axis and the density gradient into the target. This gives the standard direction of the thermally generated magnetic field — azimuthal about the laser axis, into the page at the top and out at the bottom. It would correspond to a conventional current in the direction of the laser beam.

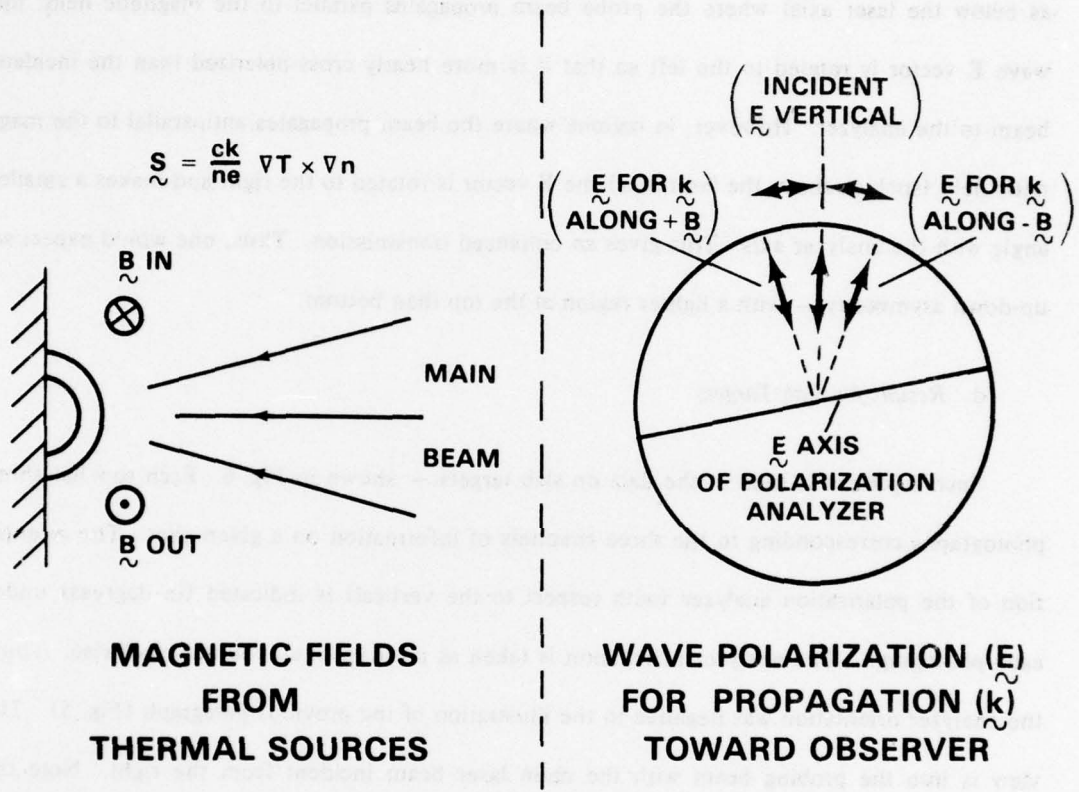


Fig. 5 — Background for understanding data: (Left) View along target surface showing direction of (azimuthal) magnetic field from a thermal source. (Right) Orientation of rotated wave electric field with respect to a tilted polarization analyzer.

Now consider the light pattern which is expected when looking through a tilted-polarization-analyzer (right-hand side of Fig. 5) at an oncoming probing laser beam which has passed out of the page through the magnetic field structure shown on the left. In regions (such as below the laser axis) where the probe beam propagates parallel to the magnetic field, the wave E vector is rotated to the left so that it is more nearly cross-polarized than the incident beam to the analyzer. However, in regions where the beam propagates antiparallel to the magnetic field (such as above the laser axis) the E vector is rotated to the right and makes a smaller angle with the analyzer axis. This gives an enhanced transmission. Thus, one would expect an up-down asymmetry — with a lighter region at the top than bottom.

d. *Results for Slab Targets*

Such a pattern is seen in the data on slab targets — shown in Fig. 6. Each row has three photographs corresponding to the three channels of information on a given shot. The orientation of the polarization analyzer (with respect to the vertical) is indicated (in degrees) under each photograph. The analyzer orientation is taken as positive when counter-clockwise. Thus, the analyzer orientation was negative in the illustration of the previous paragraph (Fig. 5). The view is into the probing beam with the main laser beam incident from the right. Note the well-localized bright regions above or below center. These correspond to light that has been Faraday rotated to give locally enhanced transmission through the analyzer. The up-down asymmetry and its reversal with analyzer orientation are consistent with thermally generated magnetic fields in the standard direction.

All of the data presented, except for the time sequence, was taken 50 psec after the peak of the main laser pulse. For the top row, the slab polystyrene (C_nH_n) target was irradiated with a single 3.5 J laser pulse- and a small but definite rotation was observed. The same target was

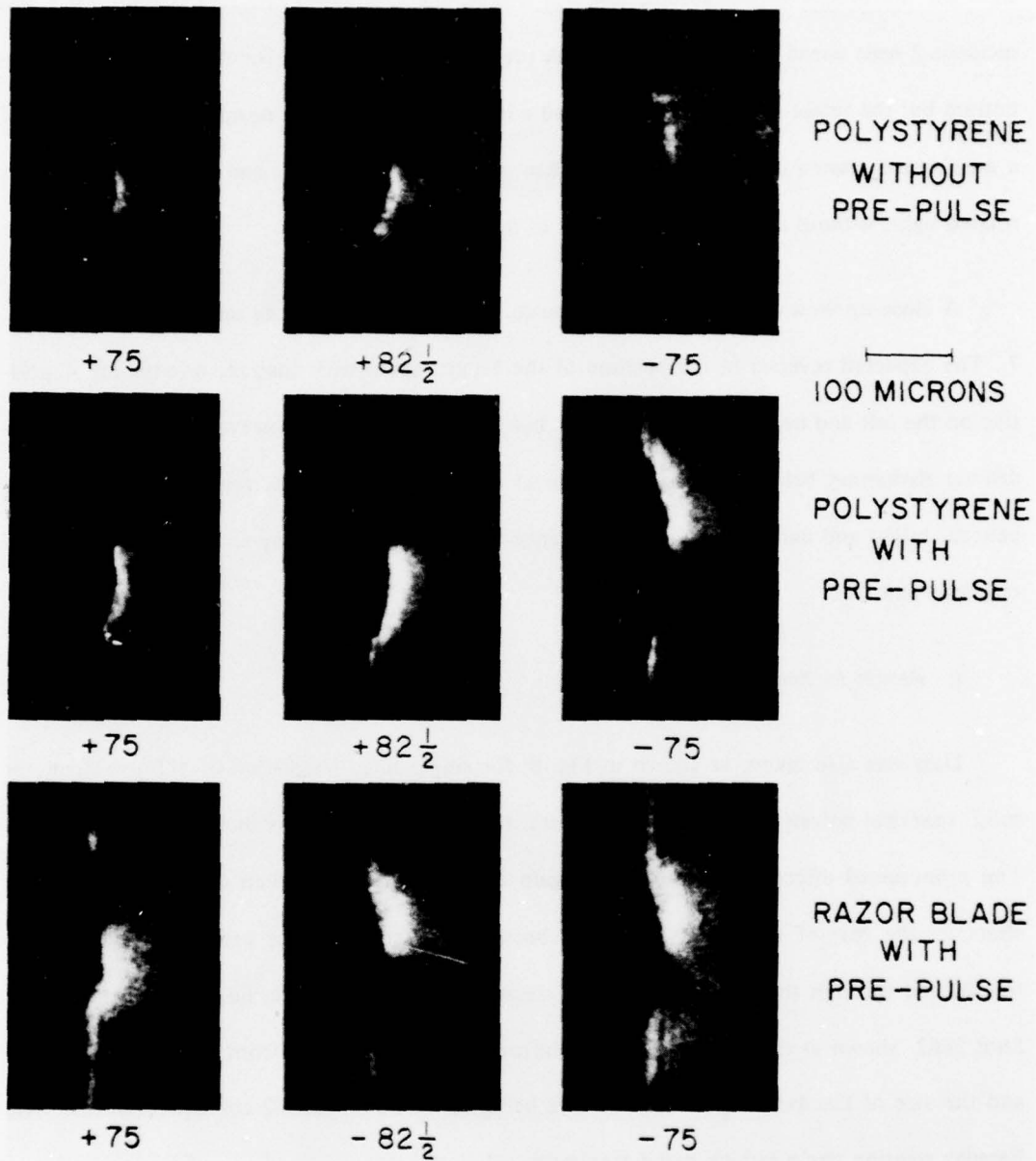


Fig. 6 - Faraday rotation photographs for slab targets, without and with pre-pulse. View is into probing beam with main laser beam incident from the right. Analyzer orientation (with respect to the incident polarization) is shown below each photograph. The position of rotated light (bright region) reverses with reversal of analyzer orientation. Probe pulse timing was +50 psec.

used for the results in the second row but a pre-pulse containing 3% of the total 4.4 J was incident 2 nsec ahead of the main pulse. A pre-pulse was also used for the shot shown at the bottom but the target — a razor blade — had a higher average atomic number. The presence of a pre-formed plasma due to the pre-pulse has increased the intensity and spatial extent of the rotated light, without affecting the direction of the magnetic field.

A close-up view of the data, with prepulse, on the slab-polystyrene target, is shown in Fig. 7. The expected reversal of the position of the bright region with analyzer orientation — positive on the left and negative on the right — has been pointed out. However, one can also see a distinct darkening below the background level opposite to the bright regions. The complete pattern, bright and dark, is convincing evidence for Faraday rotation by an azimuthally oriented magnetic field.

e. Results for Spherical Targets

Data was also taken, as shown in Fig. 8, for single-sided irradiation of 100- μm diameter solid, spherical polystyrene pellets. As before, the main laser beam is incident from the right. The pronounced effect of a pre-pulse is again evident. Structure, seen on the the pre-pulse shots, at the rear of the pellet may have been due to some of the pre-pulse energy being transmitted through the polystyrene. The magnitude of the magnetic field was calculated for Shot 3662, shown at the bottom. Density information was obtained from the interferometry⁷² and the size of the dark region (due to rays being refracted out of $f/2$ collection optics). The Faraday rotation angle (which had a maximum value of 8 degrees) and its radial variation were also used. The density was modeled with a spherical variation and the azimuthal magnetic field with a (cylindrical) axial and radial variation. The parameters were determined by matching to the experimental inputs. The magnetic field was 0.6 MG farthest away ($\sim 100 \mu\text{m}$) from the

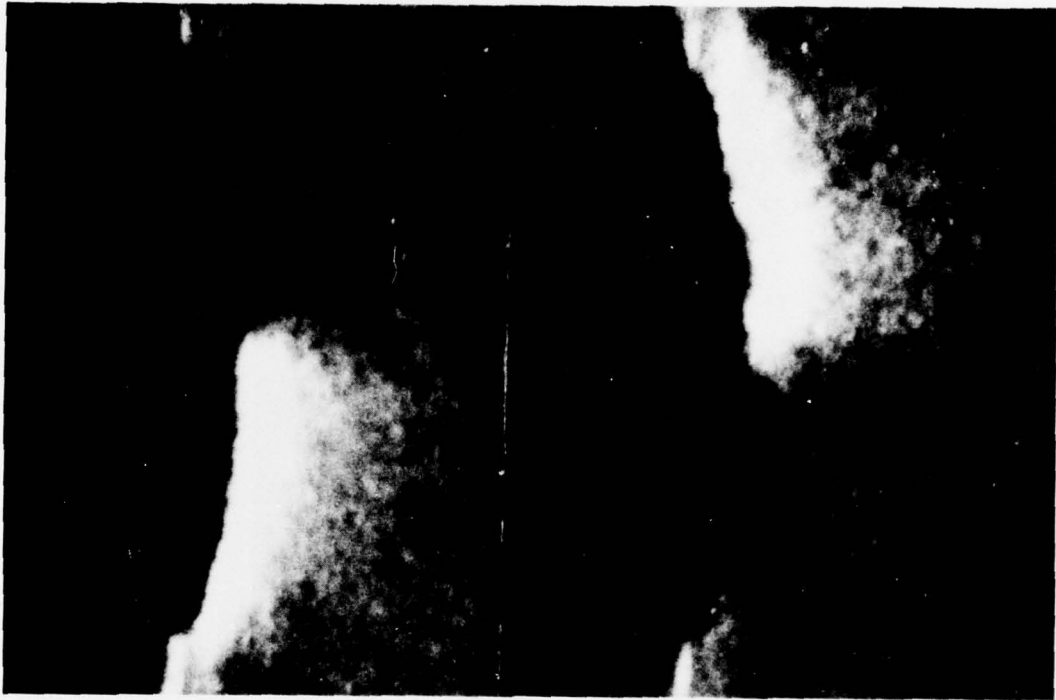


Fig. 7 - Close-up view of data, with pre-pulse, on a slab-polystyrene target. Note the darkening (below background) at a position opposite to the dark region.

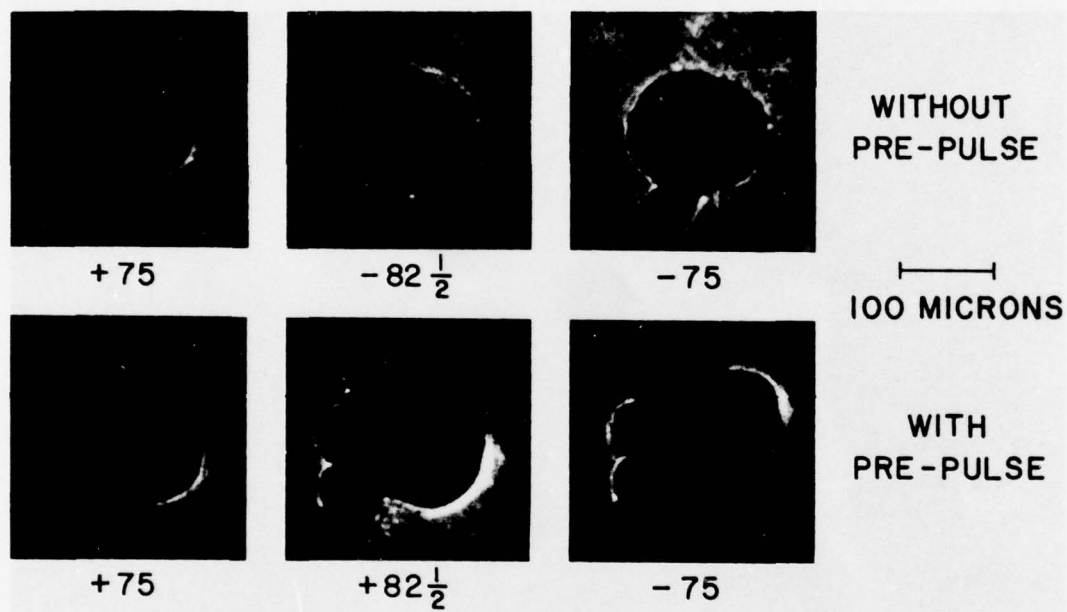


Fig. 8 — Faraday rotation photographs for spherical polystyrene targets, without and with pre-pulse. View, analyzer orientation, and timing are as in Fig. 6.

axis and was about 1.5 MG close ($25 \mu\text{m}$) to the laser axis. Such large fields (in the megagauss range) were observed in the previous NRL study¹ and have recently been observed at the Rutherford Laboratory.³

f. *Time Variation*

The photographs in Fig. 9 show how the Faraday rotated light- and, thus the magnetic field, varies with time. Time after the peak of the main laser pulse is shown in picoseconds under each photograph. The analyzer orientation (shown to the left) was reversed (from $+82\frac{1}{2}$ degrees to $-82\frac{1}{2}$ degrees) for the later times to insure that the observed pattern was actually due to rotation. The expected up-down reversal of the lighted region should be ignored so far as the time variation is concerned.

Just a hint of Faraday rotation can be seen as early as 15 psec after the main pulse. By 35 psec there was definite rotation and the maximum occurred at 50 psec — where most of the data was taken. Striations are seen at later times and may correspond to structure seen in other experiments.^{73,74} The rotated light persists as late as 450 psec where it is adjacent to the dark region.

g. *Rutherford Result*

The direction of the magnetic field remains unchanged throughout the observed period. This is consistent with the smoothing effect⁴⁴ discussed earlier, which the thermal force has on field generation. Colombant and Winsor's calculation⁴⁴ also shows a general smoothing of the spatial variations in the field. There are, in the NRL data presented here, no structures suggesting a field reversal between different spatial locations. Typical Faraday light patterns obtained at the Rutherford Laboratory³ were similar to those shown here. However, for one

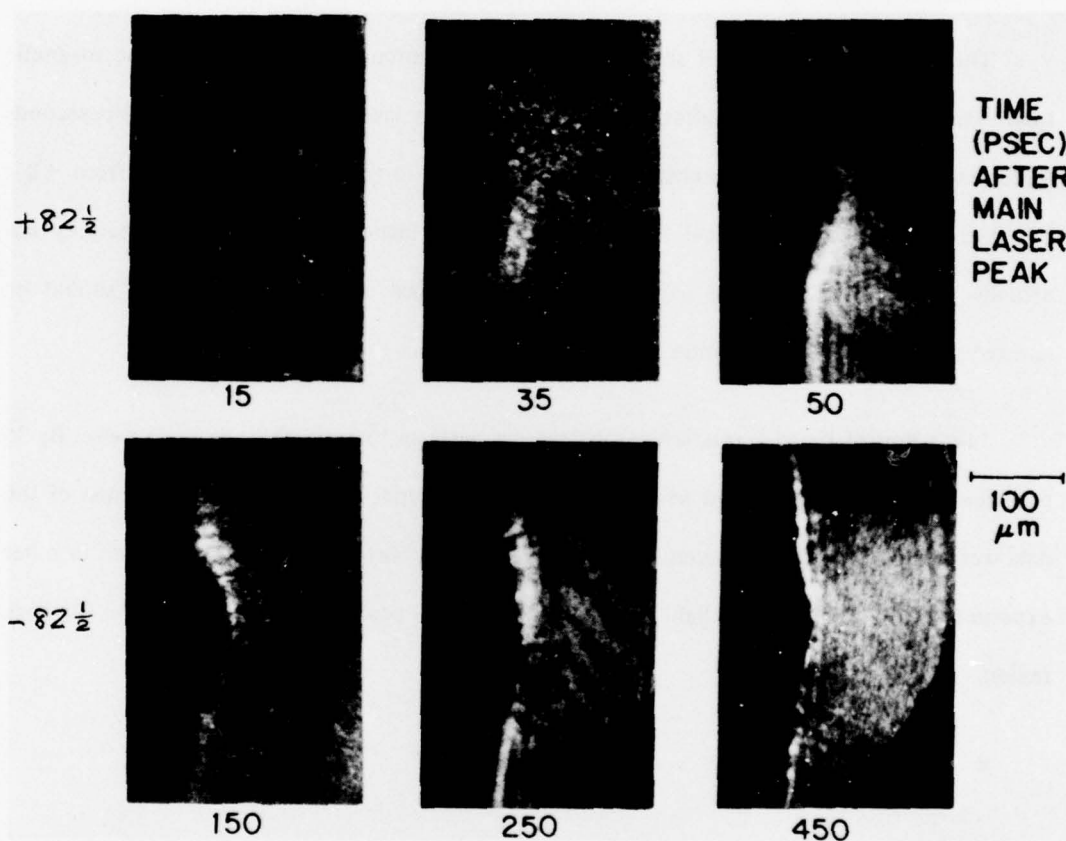


Fig. 9 - Variation of Faraday rotated light pattern with time (in psec) after peak of main laser pulse.

Rutherford shot, a photograph of the Faraday light pattern, taken with a crossed analyzer showed a double structure which corresponds to a reversed density gradient near the target. The density profile is shown at the top of Fig. 10. The Faraday rotated light pattern for this shot was rather weak and unfolding the magnetic field profile from the complicated density structure would exaggerate the uncertainty. Nevertheless, a possible field reversal is seen in the unfolded magnetic field profile — shown at the bottom. A reversed density profile and magnetic field could result from density gradient modifications by the ponderomotive forces.⁴⁶⁻⁴⁹ Such an effect is more likely in the Rutherford experiment than the NRL one since the Rutherford data was taken at a somewhat higher ($few \times 10^{16} \text{ W/cm}^2$) irradiance.

VII. CONCLUSION

The successful Faraday rotation studies have followed or accompanied a period of rapid theoretical progress. However, there has still been very little detailed comparison of experiment with theory. Some of the immediate challenges are: (1) Experimental measurements in the critical region with shorter probing wavelengths. (2) Time-resolved measurements during the laser pulse — perhaps with streak photography. (3) A combined theoretical and experimental study of magnetic field effects in pellet implosion — particularly at the lower irradiances where little work has been done.

VIII. ACKNOWLEDGMENTS

The author wishes to acknowledge useful discussions with S. E. Bodner and W. Woo. The work was supported by the U.S. Department of Energy.

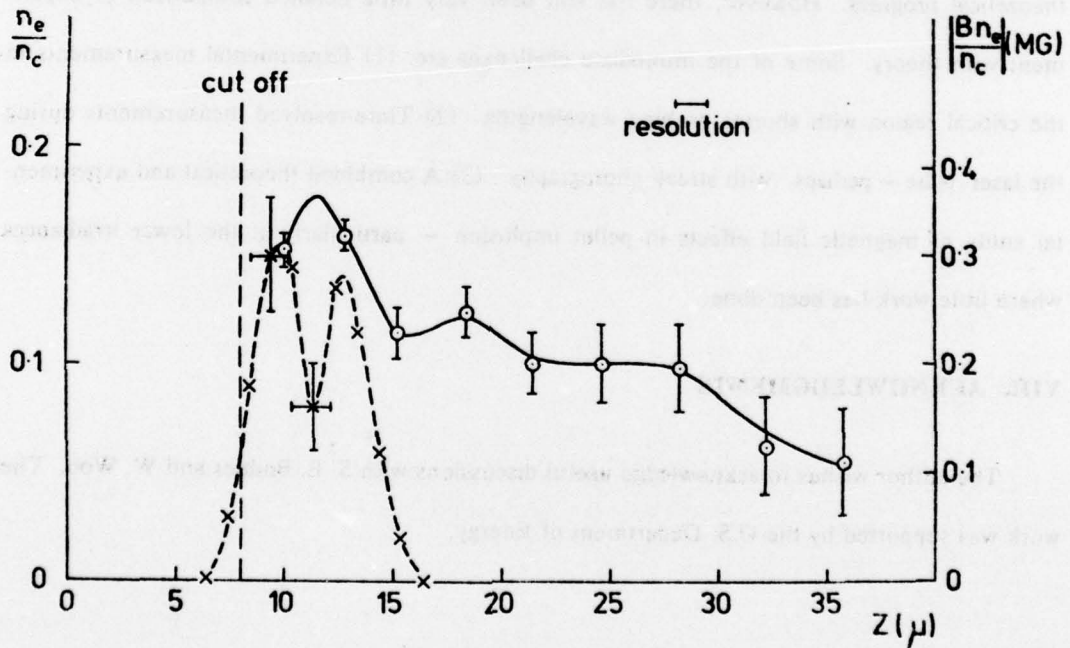
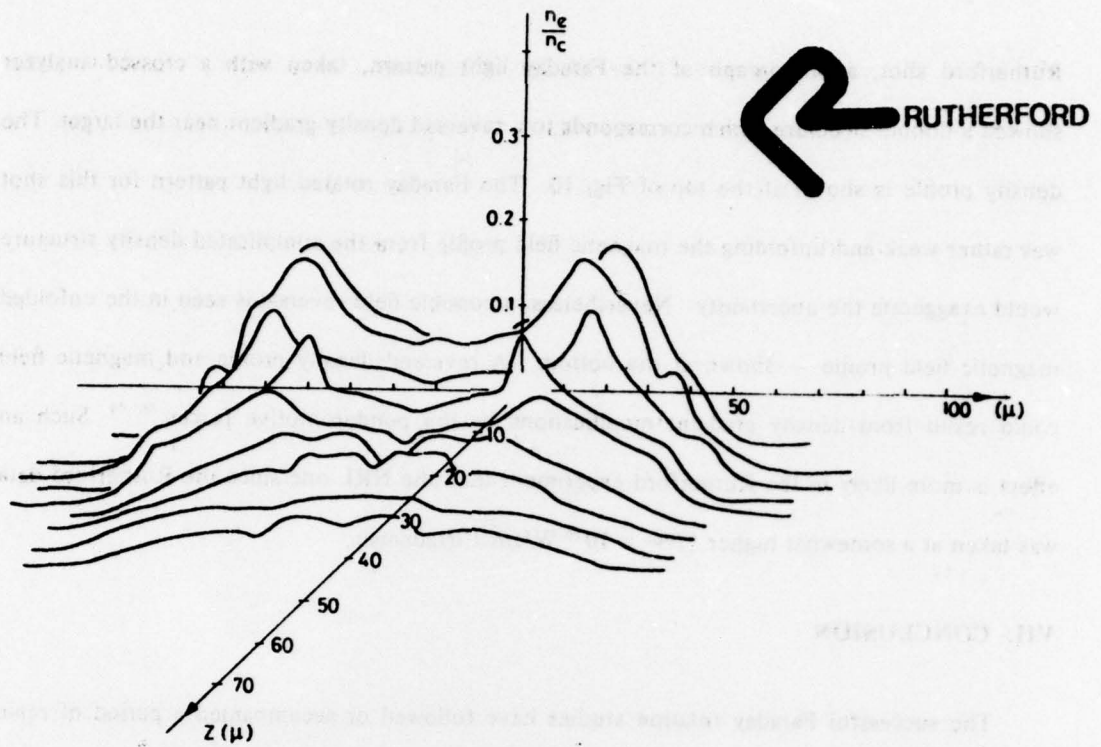


Fig. 10 - Data from Rutherford Laboratory showing reversed density gradient (top) and possible reversed magnetic field profile (bottom).

REFERENCES

1. J. A. Stamper and B. H. Ripin, Phys. Rev. Lett. **34**, 138 (1975).
2. J. A. Stamper, E. A. McLean, and B. H. Ripin, Phys. Rev. Lett. **40**, 1177 (1978).
3. A. Raven, O. Willi, and P. T. Rumsby, Phys. Rev. Lett. **41**, 554 (1978).
4. D. A. Tidman and J. A. Stamper, Appl. Phys. Lett. **22**, 498 (1973).
5. V. V. Korobkin and R. V. Serov, Zh. Eksp. Teor. Fiz., Pisma Red. **4**, 103 (1966) [JETP Lett. **4**, 70 (1966)].
6. G. A. Askar'yan, M. S. Rabinovich, A. D. Smirnova, and V. B. Studenov, Zh. Eksp. Teor. Fiz. Pisma Red. **5**, 116 (1967). [JETP Lett. **5**, 93 (1967)].
7. J. A. Stamper, K. Papadopoulos, R. N. Sudan, S. O. Dean, and E. A. McLean, and J. M. Dawson, Phys. Rev. Lett. **26**, 1012 (1971).
8. J. A. Stamper, Naval Research Laboratory Report 7411 (1972).
9. J. H. Nuckolls in LLL Semi-Annual Report, July-December 1973, UCRL-50021-73-2, pp. 76-81.
10. D. A. Tidman and L. L. Burton, Phys. Rev. Lett. **37**, 1397 (1976).
11. T. Yabe and K. Niu, J. Phys. Soc. Japan **40**, 1221 (1976).
12. D. A. Tidman, Phys. Fluids **18**, 1454 (1975).

13. J. A. Stamper, S. O. Dean and E. A. McLean in *Laser Interaction and Related Plasma Phenomena*, edited by H. Schwarz and H. Hora, (Plenum New York, 1972), Vol. 2, p. 273.
14. Fred Schwirzke in *Laser Interaction and Related Plasma Phenomena*, Edited by H. Schwarz, and H. Hora, (Plenum, New York, 1974), Vol. 3A, p. 213.
15. Erik A. Witalis in *Laser Interaction and Related Plasma Phenomena*, Edited by H. Schwarz and H. Hora (Plenum, New York 1974), Vol. 3A, p. 237.
16. J. A. Stamper, O. C. Barr, J. Davis, G. A. Doschek, C. M. Dozier, U. Feldman, B. M. Klein, W. M. Manheimer, E. A. McLean, J. M. McMahon, D. J. Nagel, D. A. Tidman, R. R. Whitlock, K. Whitney, N. K. Winsor, and F. C. Young, in *Laser Interaction and Related Plasma Phenomena*, Edited by H. Schwarz and H. Hora, (Plenum Press, New York 1974), Vol. 3B, p. 713.
17. J. A. Stamper, in *Laser Interaction and Related Plasma Phenomena*, Edited by H. Schwarz and H. Hora, (Plenum, New York 1977), Vol. 4B, p. 721.
18. R. S. Bird, L. L. McKee, F. Schwirzke, and A. W. Cooper, *Phys. Rev. A* 7, 1328 (1973).
19. L. L. McKee, R. S. Bird, and F. Schwirzke, *Phys. Rev. A* 9, 1305 (1974).
20. R. S. Case, Jr. and F. Schwirzke, *J. Appl. Phys.* 46, 1493 (1975).
21. M. G. Drouet and R. Bolton, *Phys. Rev. Lett.* 36, 591 (1976).
22. M. G. Drouet and H. Pépin, *Appl. Phys. Lett.* 28, 426 (1976).

23. M. G. Drouet, R. Bolton, G. Saint-Hilaire, P. Kieffer, Z. Szili, H. Pépin, B. Grek, A. Thi-
baudeau, and K. Trépanier, *Appl. Phys. Lett.* **29**, 469 (1976).
24. M. G. Drouet, R. Bolton, P. Kieffer, G. Saint-Hilaire, Z. Szili, H. Pépin, and B. Grek, *J.*
Appl. Phys. **48**, 2525 (1977).
25. D. F. Edwards, V. V. Korobkin, S. L. Motilyov, and R. V. Serov, *Phys. Rev. A* **16**, 2437
(1977).
26. R. Serov and M. C. Richardson, *Appl. Phys. Lett.* **28**, 115 (1976).
27. J. B. Chase, J. M. LeBlanc, and J. R. Wilson, *Phys. Fluids* **16**, 1142 (1973).
28. M. M. Widner, *Phys. Fluids* **16**, 1778 (1973).
29. N. K. Winsor and D. A. Tidman, *Phys. Rev. Lett.* **31**, 1044 (1973).
30. D. G. Colombant, K. G. Whitney, D. A. Tidman, N. K. Winsor, and J. Davis, *Phys.*
Fluids **18**, 1687 (1975).
31. C. E. Max, W. M. Manheimer, and J. J. Thomson, *Phys. Fluids* **21**, 128 (1978).
32. B. H. Ripin, P. G. Burkhalter, F. C. Young, J. M. McMahon, D. G. Colombant, S. E.
Bodner, R. R. Whitlock, D. J. Nagel, D. J. Johnson, N. K. Winsor, C. M. Dozier, R. D.
Bleach, J. A. Stamper, and E. A. McLean, *Phys. Rev. Lett.* **34**, 1313 (1975).
33. W. C. Mead, R. A. Haas, W. L. Kruer, D. W. Phillion, H. N. Kornblum, J. D. Lindl, D.
R. MacQuigg, and V. C. Rupert, *Phys. Rev. Lett.* **37**, 489 (1976).
34. R. S. Craxton and M. G. Haines, *Phys. Rev. Lett.* **35**, 1336 (1975).

35. D. A. Tidman, Phys. Rev. Lett. **32**, 1179 (1974).
36. D. A. Tidman, Phys. Rev. Lett. **35**, 1228 (1975).
37. D. A. Tidman, Phys. Fluids **19**, 321 (1976).
38. D. G. Colombant, D. A. Tidman, and N. K. Winsor, Appl. Phys. Lett. **29**, 401 (1976).
39. D. A. Tidman and R. A. Shanny, Phys. Fluids **17**, 1207 (1974).
40. B. A. Al'tercop and E. V. Mishin, Phys. Lett. **46A**, 319 (1974).
41. W. M. Manheimer and D. A. Tidman, Phys. Fluids **18**, 496 (1975).
42. R. L. McCrory, Private communication.
43. G. J. Pert, J. Plasma Physics **18**, 227 (1977).
44. D. G. Colombant and N. K. Winsor, Phys. Rev. Lett. **38**, 697 (1977).
45. J. A. Stamper, Phys. Fluids **19**, 758 (1976).
46. D. W. Forslund, J. M. Kindel, Kenneth Lee, E. L. Lindman, and R. L. Morse, Phys. Rev. A **11**, 679 (1975).
47. T. P. Donaldson and J. J. Spalding, Phys. Rev. Lett. **36**, 467 (1976).
48. D. W. Forslund, J. M. Kindel, and K. Lee, Phys. Rev. Lett. **39**, 284 (1977).
49. D. T. Attwood, D. W. Sweeney, J. M. Auerbach, and P. H. Y. Lee, Phys. Rev. Lett. **40**, 184 (1978).

50. W. Woo and J. S. DeGroot, *Phys. Fluids* **21**, 124 (1978). A generalized version appears in U. Cal. (Davis) Report No. PRG-23, Rev. 3, June 6, 1978 (to be published in the *Physics of Fluids*).
51. J. A. Stamper and S. E. Bodner, *Phys. Rev. Lett.* **37**, 435 (1976).
52. J. A. Stamper, *Appl. Phys. Lett.* **31**, 574 (1977).
53. B. Bezzerides, D. F. DuBois, D. W. Forslund, and E. L. Lindman, *Phys. Rev. Lett.* **38**, 495 (1977).
54. J. A. Stamper and D. A. Tidman, *Phys. Fluids* **16**, 2024 (1973).
55. J. J. Thomson, C. E. Max, and K. Estabrook, *Phys. Rev. Lett.* **35**, 663 (1975).
56. E. Schmutzer and B. Wilhemi, *Plasma Physics* **19**, 799 (1977).
57. W. Woo, K. Estabrook, and J. S. DeGroot, *Phys. Rev. Lett.* **40**, 1094 (1978).
58. K. Nishihara, Y. Ohsawa, K. Mima, and T. Tange, *Phys. Fluids* **19**, 1833 (1976).
59. T. Speziale and P. J. Catto, to be published (November 1978) in the *Physics of Fluids*.
60. J. R. Cary and A. N. Kaufman, *Phys. Rev. Lett.* **39**, 402 (1977).
61. W. F. DiVergilio, A. Y. Wong, H. C. Kim, and Y. C. Lee, *Phys. Rev. Lett.* **38**, 541 (1977).
62. A. Raven and P. T. Rumsby, *Phys. Lett* **60A**, 42 (1977).
63. S. P. Obenschain and N. S. Luhmann, Jr., to be published in *Physical Review Letters*.

64. W. L. Kruer and K. Estabrook, *Phys. Fluids* **20**, 1688 (1977).
65. R. B. White and F. F. Chen, *Plasma Physics* **16**, 565 (1974).
66. C. Grebogi, C. S. Liu, and V. K. Tripathi, *Phys. Rev. Lett.* **39**, 338 (1977).
67. W. Woo, K. Estabrook and J. S. DeGroot, *Phys. Rev. Lett.* **40**, 1094 (1978).
68. E. A. McLean, J. A. Stamper, R. H. Ripin, H. R. Griem, J. M. McMahon, and S. E. Bodner, *Appl. Phys. Lett.* **31**, 825 (1977).
69. D. T. Attwood, in *Proceedings of the Twelfth International Congress on High Speed Photography*, Toronto, 1976 (Society of Photo-Optical Instrumentation Engineers, Redondo-Beach, Calif. 1976), Vol. 97, p. 413. Later studies (private communication) at 100 psec and 10^{15} W/cm² also showed no fields larger than 100 kG.
70. D. C. Montgomery and D. A. Tidman, *Plasma Kinetic Theory*, (McGraw Hill, New York, 1964), p. 123, Note that their Ω_i for electrons is $-\omega_c$, here.
71. R. H. Lehmburg and J. A. Stamper, *Phys. Fluids* **21**, 814 (1978).
72. E. A. McLean, to be published.
73. G. A. Doschek, U. Feldman, P. G. Burkhalter, T. Finn, and W. A. Feibelman, *J. Phys. B: Atom. Molec. Phys.* **10**, L745 (1977). Localized ion emission observed in spectroheliograms.
74. B. Grek, F. Martin, H. Pepin, G. Mitchel, T. W. Johnston, and F. Rheault; to be published (1978) in *Physical Review Letters*. Fine-scale density structure observed by interferometry.